nature research
https://doi.org/10.1038/s41550-020-1197-x

Supplementary information

Lunar regolith and substructure at Chang'E-4 landing site in South Pole–Aitken basin

In the format provided by the authors and unedited

Supplementary Information for

Lunar regolith and substructure at Chang'E-4 landing site in South Pole-Aitken basin

Jinhai Zhang[1†], Bin Zhou[2†], Yangting Lin[1]*, Meng-Hua Zhu[3†], Hanjie Song[4], Zehua Dong[2], Yunze Gao[2], Kaichang Di[5], Wei Yang[1], Hongyu Lin[6], Jianfeng Yang[7], Enhai Liu[8], Lei Wang[4], Yi Lin[1], Chao Li[1], Zongyu Yue[5], Zhenxing Yao[1], Ziyuan Ouyang[9]

[1]Key Laboratory of Earth and Planetary Physics, Institute of Geology and Geophysics, Chinese Academy of Sciences, Beijing 100029, China

[2]Key Laboratory of Electromagnetic Radiation and Detection Technology, Institute of Electronics, Chinese Academy of Sciences, Beijing 100190, China

[3]State Key Laboratory of Lunar and Planetary Sciences, Macau University of Science and Technology, Taipa, Macau, China

[4]National Space Science Center, Chinese Academy of Sciences, Beijing 100190, China

[5]State Key Laboratory of Remote Sensing Science, Institute of Remote Sensing and Digital Earth, Chinese Academy of Sciences, Beijing 100101, China

[6]Beijing Institute of Space Mechanics & Electricity, Beijing 100076, China

[7]Xi'an Institute of Optics and Precision Mechanics, Chinese Academy of Sciences, Xi'an 710119, China

[8]Institute of Optics and Electronics, Chinese Academy of Sciences, Chengdu 610209, China

[9]Institute of Geochemistry, Chinese Academy of Sciences, Guiyang 550002, China

*correspondence to: linyt@mail.iggcas.ac.cn; [†]equal contributions to this work.

This file includes:

Supplementary Figure 1 to 5

Supplementary Table 1

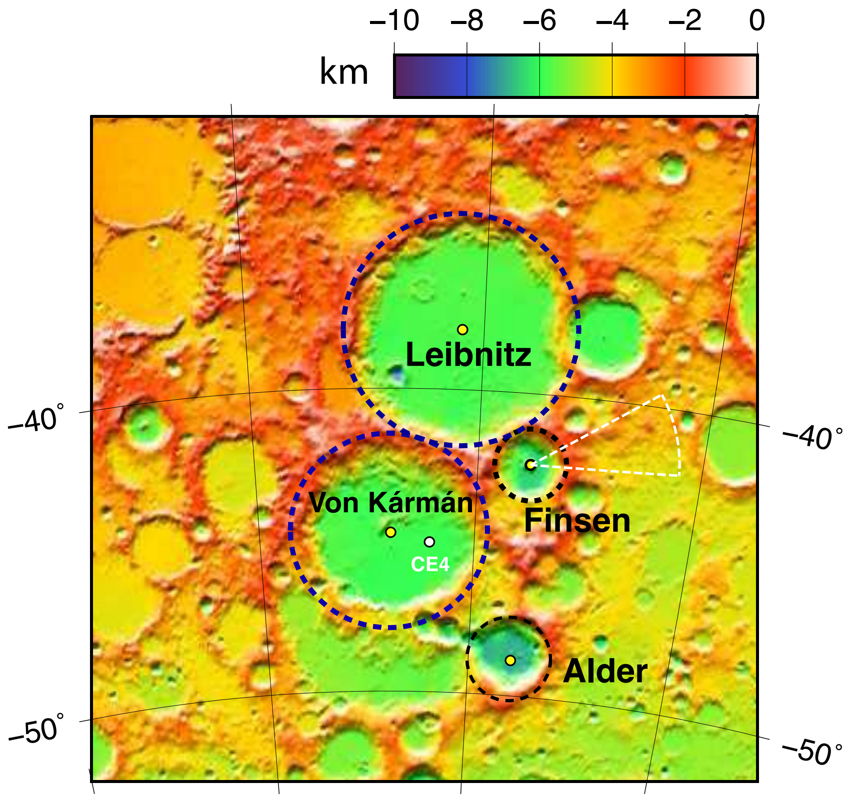

Supplementary Figure 1. The topographic maps of craters surrounding the CE-4 landing site. The highlighted craters are the Leibnitz, Finsen, Alder, and Von Kármán craters. The circles represent the rims of the craters while the yellow points represent the crater centers. The white point represents the CE-4 landing site. For the Finsen crater, we average the profiles in a crater-centered projection over the white region to get the average profile of the topography around the crater (Supplementary Figure 2). The image is overlaid by a shaded relief map derived from surface topography in an azimuthal projection.

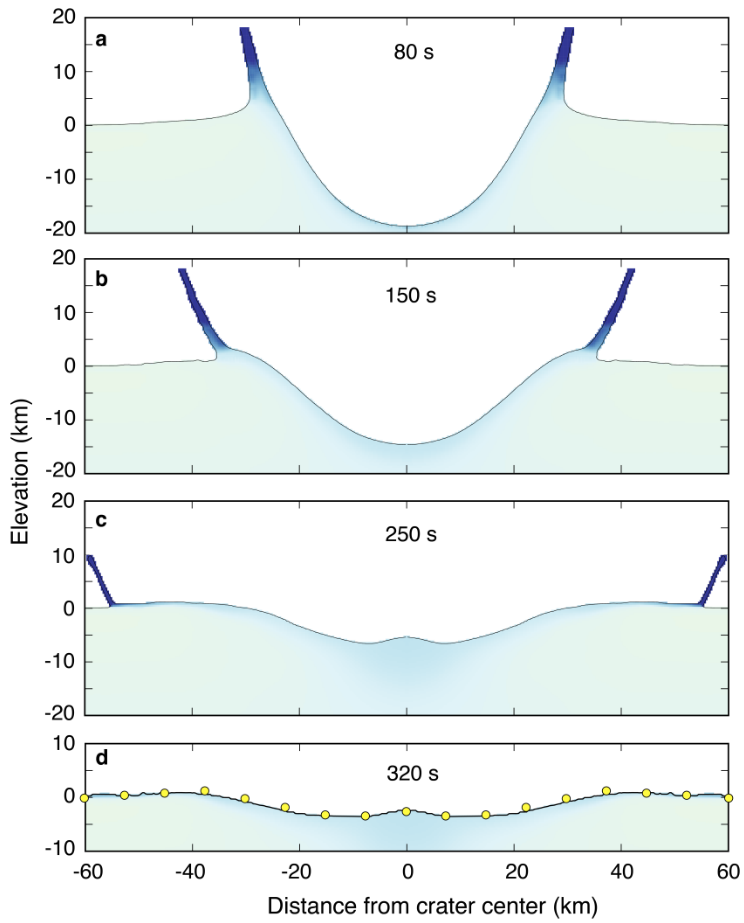

Supplementary Figure 2. The snapshots of Finsen crater formation process at different times (a~d). The impactor diameter is 6.2 km with an impact velocity of 15 km s^{-1}. The impact produces a structure with a diameter of ~78 km, similar to the size of the Finsen crater. The yellow dots in (**d**) represent the relative elevation of the Finsen crater derived from the LOLA observations (Supplementary Fig. 1). The color in each snapshot represents the relative density during the impact cratering formation in which the dark color represents the lower density material than the material represented by the light color. The time in each snapshot represents the modeling time.

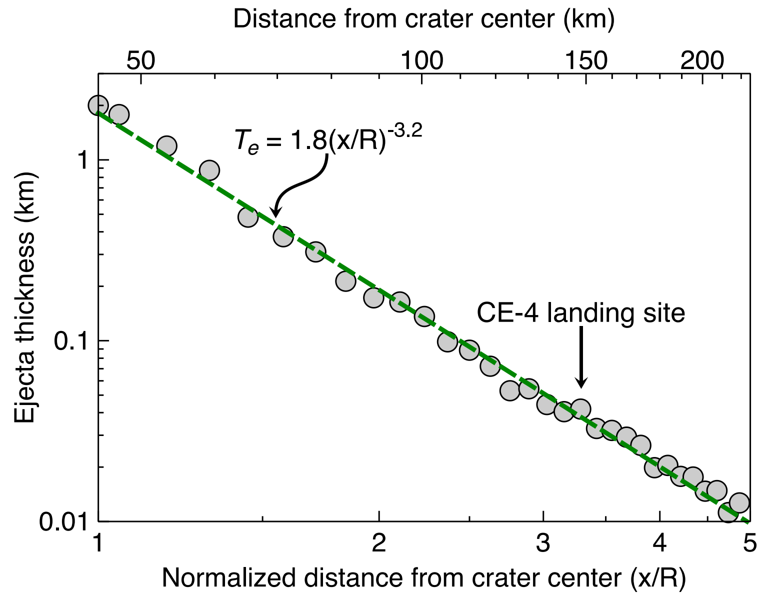

Supplementary Figure 3. The ejecta thickness of simulated Finsen crater. The points represent the simulated ejecta thickness; the green dashed line represents the fitted power law function with an exponent of -3.2. The CE-4 landing site is about 140 km from the center of the Finsen crater.

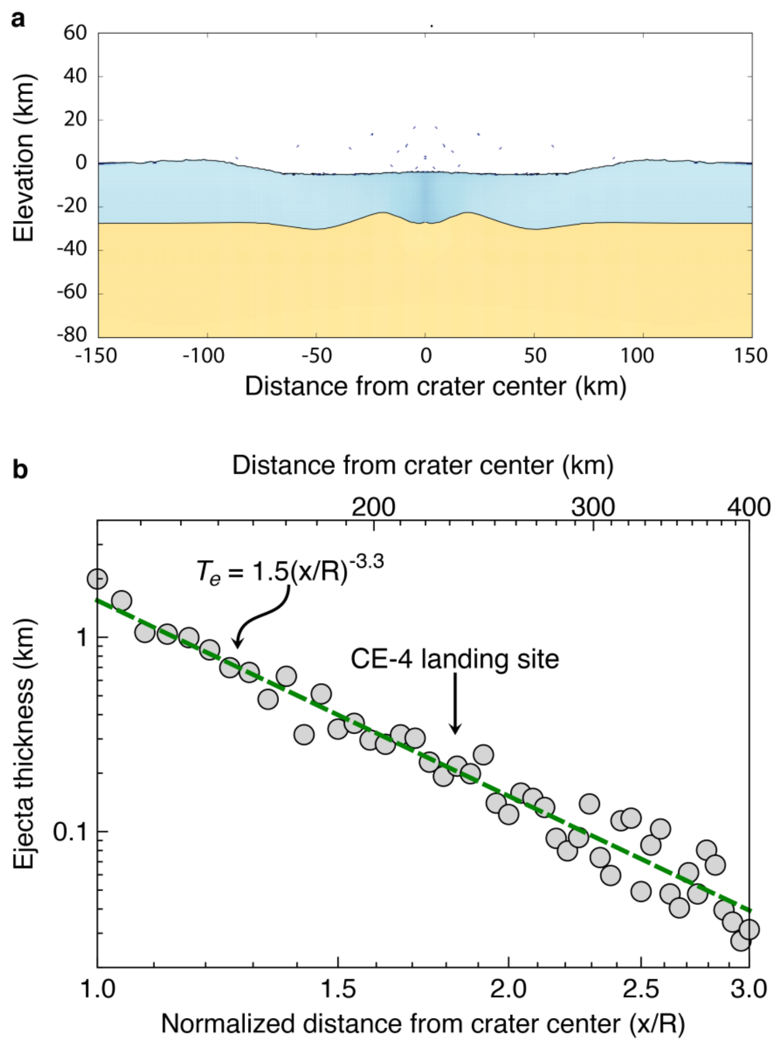

Supplementary Figure 4. The final structure of the Leibnitz-sized crater (**a**) **and its ejecta thickness distribution** (**b**)**.** The crust thickness was assumed to be ~20 km (*52*). The impactor diameter is 14 km with an impact velocity of 16 km s^{-1}. The points in (**b**) represent the simulated ejecta thickness and the green dashed line represents the fitted power law function with an exponent of -3.3. The CE-4 landing site is about 240 km from the center of Leibnitz crater. In (**a**) the blue color represents the crustal material whereas the yellow color represents the mantle material.

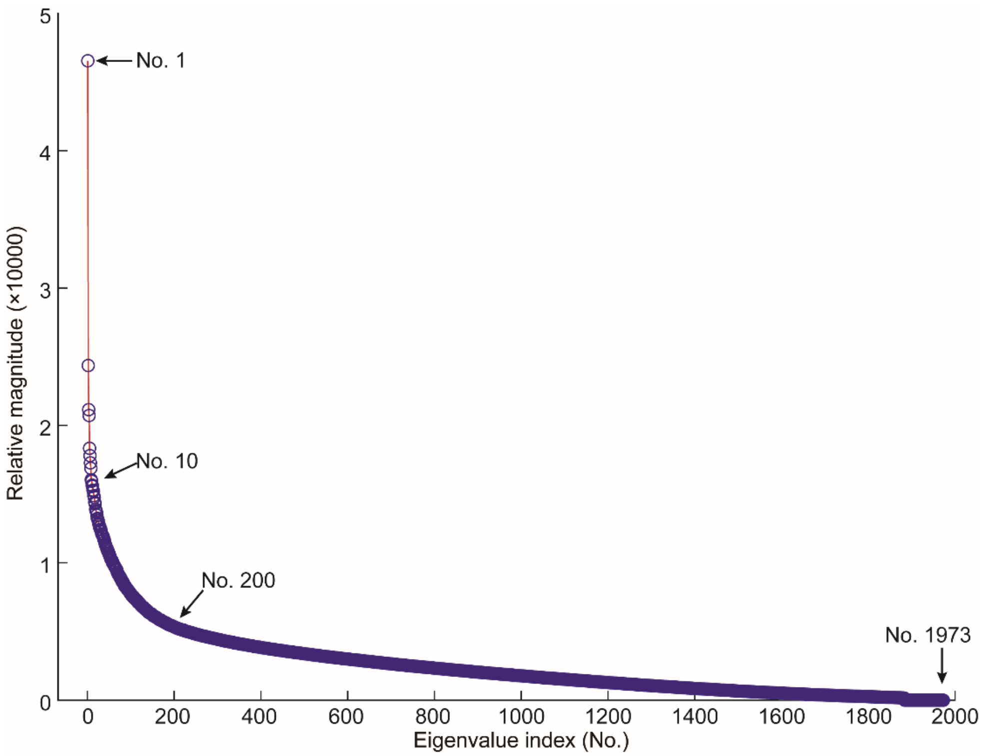

Supplementary Figure 5. Singular values of low-frequency LPR channel. The singular value decomposition of low-frequency LPR channel is shown in Extended Data Figure 6.

Supplementary Table 1. Material input parameters used for the iSALE models.

Parameter	Dunite	Gabbro
Equation of state	Tillotson	ANEOS
Poisson’s ration	0.25	0.25
Intact cohesive strength (MPa)	5.07	10
Intact friction coefficient	1.58	2.0
Intact strength limit (GPa)	3.26	2.5
Damaged cohesive strength (MPa)	0.1	0.01
Damaged friction coefficient	0.63	0.7
Melt temperature (K)	1373	1673
Constant in Simon approximation	1.52	6
Exponent in Simon approximation	4.05	3
Acoustic Fluidization decay time constant	300	300
Acoustic Fluidization viscosity constant	0.04	0.4